Ultrahigh water permeation with high multivalent metal ions rejection rate through graphene oxide membranes

Fangfang Dai
Zhejiang A & F University
Feng Zhou
Key Laboratory of Radiation Monitoring of Zhejiang Province
Junlang Chen
Zhejiang A & F University
Shanshan Liang
East China University of Science and Technology
Liang Chen (liangchen@zafu.edu.cn)
Zhejiang A & F University
Haiping Fang
Shanghai Institute of Applied Physics, Chinese Academy of Sciences, Shanghai 201800
https://orcid.org/0000-0002-3496-9923

Article

Keywords: Ultrahigh water permeation, graphene oxide (GO) membranes, molecular permeation, high multivalent metal ions rejection rate

Posted Date: October 5th, 2020

DOI: https://doi.org/10.21203/rs.3.rs-74370/v1

Version of Record: A version of this preprint was published at Journal of Materials Chemistry A on January 1st, 2021. See the published version at https://doi.org/10.1039/D1TA00647A.

Abstract

Graphene oxide (GO) membranes show exceptional molecular permeation properties and have gained tremendous attention in the area of wastewater treatment. However, they still suffer from some limitations, such as low water permeance when the ion rejection rate is at a satisfactory level and unstable performance. Here, we develop a sort of GO membrane that exhibits ultrahigh water permeance up to 75.2 L m^{-2} h^{-1} bar^{-1} while still maintaining a high rejection rate of 99.9% for multivalent metal ions. Importantly, of all state-of-the-art nanofiltration membranes, this is the most permeable membrane with a satisfactory level of rejection rate for multivalent ions. Furthermore, the GO membrane has outstanding stability over long-time operation. Our work provides a simple way to fabricate GO membranes with outstanding water purification performance.

Introduction

Water purification is an attractive pathway to fresh water[1,2], and membrane technologies, one of the most important energy-efficient and environmentally friendly strategies for water treatment, have attracted intensive interest in recent years[3,4]. An ideal water treatment membrane should exhibit key performance benchmarks, including high water permeance with an efficient rejection rate and good stability[5-7].

Graphene oxide (GO)—made from partially oxidized, stacked sheets of graphite[8]—is considered to be an ideal nano-filtration membrane material for removing nanoscale solutes from water, due to its unique two-dimensional structures[9-15], robust chemical stability[16], and uniform and narrow pore size distribution for efficient separation[17-22]. GO membranes have been shown to have potential for a variety of applications[23-26], especially for water purification and desalination, due to their precise ionic and molecular sieving capability in aqueous solutions[27-33]. However, a low water permeance when the ion rejection rate is large enough, together with unstable performance, limits the practical applications of GO membranes for water purification[34-38]. For example, for some typical multivalent ions of Pb^{2+}, Ni^{2+}, Zn^{2+}, and Cd^{2+}, although the modified GO membranes show high rejection rates of about 95%, 96%, 97% and 90%, respectively, the pure water permeance is only ~5.0 L m^{-2} h^{-1} bar^{-1})[39]. Recently, a large-area graphene nanomesh/single-walled carbon nanotube hybrid membrane also possesses high rejection rates of about 92% for Mg^{2+}, while the pure water permeance of the membrane is still moderate (20.6 L m^{-2} h^{-1} bar^{-1})[40].

Here, we develop a sort of GO membrane that achieves an unprecedented water permeance while maintaining an ultrahigh ion rejection rate for multivalent metal ions. The water permeance reaches up to 75.2 L m^{-2} h^{-1} bar^{-1}, which is about one or two orders of magnitude higher than the permeances through most GO membranes reported previously[18,37,38,41]. Remarkably, the GO membrane has superior filtration performance compared to other nanofiltration membranes, as the highest water permeance is about 62 L m^{-2} h^{-1} bar^{-1} with a rejection rate of 98 % for multivalent metal ions very recently[42]. Also, the GO

membranes have outstanding stability. Thus, this work provides a simple avenue to fabricate GO membranes with exceptional filtration performance.

Results

As illustrated in Fig. 1(a), GO membranes were prepared from 40 mL, 7.5 mg/L GO suspensions on mixed cellulose ester (MCE) substrates using vacuum filtration. Then, 5~500 mg/L different salts ($FeCl_3$, $Pb(NO_3)_2$, $ZnSO_4$ and $CuSO_4$) solutions were added to the feed side, respectively. Under a pressure of 1 bar, the salt solutions were filtered through GO membranes. Filtrates were collected after 20 min when the filtration process became steady. Water permeances were calculated by measuring the time required to collect 30 mL filtrate, and the corresponding concentrations of $FeCl_3$, $Pb(NO_3)_2$, $ZnSO_4$ and $CuSO_4$ in the filtrate were measured using inductive coupled plasma-optical emission spectrometry (ICP-OES). Rejection rates were calculated from the concentration of feed and permeate solution (see details in Methods). Three parallel permeation tests were performed to obtain averaged values of water permeance and rejection rate.

As shown in Fig. 1(b), the water permeance was 75.2 L m^{-2} h^{-1} bar^{-1} with a high rejection rate of 99.9% for a 5 mg/L $FeCl_3$ 1 bar. Increasing the concentration of the $FeCl_3$ solution to 50 mg/L, 250 mg/L and 500 mg/L, the permeances dropped to 63.5 L m^{-2} h^{-1} bar^{-1}, 54.9 L m^{-2} h^{-1} bar^{-1} and 48.2 L m^{-2} h^{-1} bar^{-1}, with corresponding rejection rates of 98.9%, 90.1% and 89.8%, respectively (see Supplementary Fig. S2 in Supporting Information). These permeances are one to two orders of magnitude higher than those of most GO membranes reported previously[18,37,38,41] (see details in Supporting Information section PS 3) . We note that the highest water permeance previously reported very recently for state-of-the-art nanofiltration membranes is about 62 L m^{-2} h^{-1} bar^{-1} with only a 98% rejection rate[42], as shown in Fig. 1(c) and Table S1 in Supporting Information section PS 3. Thus, the water permeances we obtained are much superior to the permeances of all other nanofiltration membranes with reasonable rejection rates for 50~1000 mg/L multivalent metal ion solutions. In addition, for other multivalent ions of $CuSO_4$, $Pb(NO_3)_2$ and $ZnSO_4$, the water permeances were 56.6 L m^{-2} h^{-1} bar^{-1}, 46.6 L m^{-2} h^{-1} bar^{-1}, and 48.7 L m^{-2} h^{-1} bar^{-1} with corresponding rejection rates of 97.8%, 86.9%, and 83.0%, respectively. Although these permeances and rejection rates are lower than the permeance for $FeCl_3$ at the same concentration, they are still superior to most other membranes, as shown in Fig. 1(b), (c), and the Table S1 in Supporting Information section PS 3. Thus, the GO membranes in the present work exhibit ultrahigh water permeances with high rejection rates for multivalent ions.

The GO membranes also showed outstanding stability with superior performance. Fig. 1(e) shows that the water permeance decreases from 95.5 L m^{-2} h^{-1} bar^{-1} and reaches a stable value of 75.2 L m^{-2} h^{-1} bar^{-1} within 100 min, while the corresponding rejection rate is maintained at more than 97% for 5mg/L $FeCl_3$. We noted that the feed salt concentration continuously increased in the dead-end filtration set-up. In addition, the increased salt concentration (concentration polarization) could affect the membrane

performance. Therefore, a semi-continuous process was employed for the long-term operation experiment of the high-concentration solution filtered by the GO membranes[43]: the surface and filtration cleaning of the GO membranes by DI water were performed before the next filtration (see details in Supporting Information section PS 7). The water permeances slightly decreased slightly from 49.0 L m^{-2} h^{-1} bar^{-1} to 46.5 L m^{-2} h^{-1} bar^{-1}, while the corresponding rejection rates increased from 85.0% to 96.4%, showing an outstanding stability with superior filtration performance of the GO membranes (see Fig. S5 in Supporting Information section PS7). We believe that the increase in the rejection rate and the slight decrease in the water permeance were mainly due to the improved self-assembly and more compacted structures between the GO sheets under the long-term vacuum filtration conditions.

In addition, we analysed the the ions adsorption by the GO membranes in our filtration experiments[44]. As shown in Fig. 2, the adsorption efficiency of the GO membranes for $ZnSO_4$, $CuSO_4$, $FeCl_3$, and $Pb(NO_3)_2$ were 13%, 19%, 26%, and 42%, respectively. As mentioned above, the rejection rates of the GO membranes were 83% ~ 99.9% (see Fig. 1(b)), which are much higher than 13% ~ 42% removed by adsorption. These results indicate that the significant effect on the removal multivalent ions at a low concentration of 5 mg/L is mainly due to rejection by the GO membranes, even though the adsorption effect cannot be negligible. Further, we performed adsorption experiments using $FeCl_3$ solution with a high concentration of 500 mg/L. As shown in Fig. S6 in Supporting Information section PS8, the $FeCl_3$ solution with 500 mg/L showed stable concentration for over 120 min. The removal rate by adsorption was < 4%. Considering the rejection rate for 500 mg/L $FeCl_3$ solution was 89.8 %. Thus, for the high salts concentrations, the salts removal are almost entirely attributed to the rejection rather than adsorption by the GO membranes, which was further confirmed by the mass balance experiment (see details in Supporting Information section PS 9).

Our previous experimental studies showed that the order in which the GO membrane is exposed to ions is important for efficient ion sieving[41]. One type of ions enter the membrane first, controlling the interlayer spacing and potentially excluding other cations that require a larger interlayer spacing, or allowing other hydrated cations with smaller sizes to pass through. Thus, we performed additional permeation experiments with GO membranes using $ZnSO_4$ or $FeCl_3$ as controlled ions, which are denoted as $ZnSO_4$-controlled GO membranes or $FeCl_3$-controlled GO membranes. Explicitly, 20 mL, 5 mg/L $ZnSO_4$ or $FeCl_3$ solutions were first added to the feed side and then filtered at a pressure of 1 bar. Subsequently, salt solutions including 5 mg/L $ZnSO_4$ or $FeCl_3$ with 5 mg/L target salts ($Pb(NO_3)_2$, $CuSO_4$, $FeCl_3$, or $ZnSO_4$) were added to the feed side, and the mixed salt solutions were filtered through GO membranes at the same pressure. The filtrates of the mixed solutions were collected after 20 min when the filtration process became steady, and the concentrations of target testing ions in the filtrates were measured. Rejection rates were calculated from the concentrations of feed and permeate solutions (see details in Methods).

We found that $ZnSO_4$-controlled GO membranes and $FeCl_3$-controlled GO membranes had different rejection performance. The $ZnSO_4$-controlled GO membranes showed high rejection rates of 99.6%, 95.1%, and 92.6% for $FeCl_3$, $Pb(NO_3)_2$, and $CuSO_4$, with corresponding water permeances of 44.2 L m^{-2}

h^{-1} bar^{-1}, 42.9 L m^{-2} h^{-1} bar^{-1}, and 24.2 L m^{-2} h^{-1} bar^{-1}, respectively (see Fig. 3(a)). In contrast, $FeCl_3$-controlled GO membranes have rejection rates for $Pb(NO_3)_2$, $CuSO_4$, and $ZnSO_4$ of only 47.6%, 39.8%, and 24.8% with corresponding water permeances of 61.9 L m^{-2} h^{-1} bar^{-1}, 42.9 L m^{-2} h^{-1} bar^{-1}, and 44.7 L m^{-2} h^{-1} bar^{-1}, respectively (see Fig. 3(c)). The rejection rates for the $FeCl_3$-controlled GO membranes are much lower than the rejection rates for the $ZnSO_4$-controlled GO membranes.

To illustrate the underlying physical mechanism, the interlayer spacings of the GO membranes fabricated in the present work were analyzed by X-ray diffraction. As shown in Fig. 1(d), the interlayer spacings indicated by the Bragg peaks of X-ray diffraction) were 15.8 ± 0.1 Å, 15.7 ± 0.1 Å, 15.3 ± 0.1 Å, and 15.2 ± 0.1 Å for GO membranes immersed in only $FeCl_3$, $Pb(NO_3)_2$, $CuSO_4$, or $ZnSO_4$ solutions, respectively. These values are all about 3 Å larger than the interlayer spacings of the GO membranes prepared by the conventional drop-casting method[41,45,46] (see details in Methods), which were 13.1 Å, 13.0 Å, 13.0 Å, and 12.8 Å for the drop-casting GO membranes immersed in $FeCl_3$, $Pb(NO_3)_2$, $CuSO_4$, and $ZnSO_4$ solutions. The large interlayer spacings of the GO membranes prepared by the present method can be further demonstrated by the interlayer spacing of the GO membrane immersed in pure water, which was 16.2 Å (Fig. 1(d)), this is also ~3 Å larger than the interlayer spacing of 13.0 Å for the GO membrane fabricated by the drop-casting method immersed in pure water, as reported earlier[41]

Discussion

We think that the larger interlayer spacings of the GO membranes in the present work are attributed to the fabrication process without drying treatment. We note that a drying treatment process was previously used during the fabrication of GO membranes prepared by the drop-casting method[41,45,46]. During the drying treatment, the water molecules between the GO sheets are lost, which leads to a reduction in spacing between the GO sheets. In some parts of the spacings between two GO sheets, there is no water, which causes direct contact between the two GO sheets, and thus induces the π-π stacking[47] formed between the aromatic rings in the upper and lower GO sheets. Due to those π-π stackings, it is very difficult for water molecules to enter the spacings between the GO sheets when the GO membranes prepared by the conventional drop-casting method are again immersed in an aqueous solution. Thus, due to the drying treatment, some spacings in the GO membranes fabricated by the drop-casting method are very small. As a result, the distribution of the spacings between the GO sheets in membranes fabricated by the conventional drop-casting method shifts toward small values due to the drying treatment. In contrast, the GO membranes in the present work have larger spacings due to the lack of the drying treatment. We note that the interlayer spacing corresponds to the largest distribution of the spacings. Therefore, the GO membranes in the present work have larger interlayer spacings.

Considering that the sizes of the hydrated multivalent metal ions are much larger than the sizes of the hydrated anions, the hydrated anions should not pass through the membrane due to the electrostatic interactions between the cations and the anions when the cations are rejected. To demonstrate that the effect of anions in these multivalent ions rejection is negligible, we further performed ions permeation

tests with different anions. Taking Fe^{3+} as an example, the three Fe^{3+} salts solutions with different anions (Cl^-, NO_3^-, and SO_4^{2-}) have been tested, as shown in Supporting Information section PS 10. The water permeances for three Fe^{3+} salts solutions with different anions of Cl^-, NO_3^-, and SO_4^{2-} were 75.1 L m^{-2} h^{-1} bar^{-1}, 71.7 L m^{-2} h^{-1} bar^{-1}, and 67.3 L m^{-2} h^{-1} bar^{-1}, with corresponding rejection rates of 99.5%, 97.7%, and 98.3%, respectively. Therefore, the differences in the water permeances and rejection rates were negligible. Thus, the anions have less contribution to the high water permeances for multivalent metal ions rejection using the GO membrane.

One may argue that the GO membranes in the present work with larger interlayer spacings still have high rejection rates for the multivalent ions. Clearly, the hydrated ions fix the spacings between the neighboring GO sheets due to the strong hydrated cation-π interactions[41,48]. The key for ion rejection is the gate size determined by these hydrated ions[10]. The interlayer spacing, corresponding to the largest distribution of the spacings in the GO membranes, is not the gate for the ion rejection but usually correlates with the gate size[10]. We note that, when the hydrated multivalent ions enter the space between GO sheets, the hydration structures of the multivalent ions will be distorted due to the strong hydrated cation-π interactions from the DFT calculations (see details in Methods), we observed that, when the hydrated multivalent ions enter the space between GO sheets, the hydration structures of the multivalent ions are distorted due to the strong hydrated cation-π interactions. The stable optimized geometries of hydrated Fe^{3+}- $(H_2O)_6$ and hydrated Fe^{3+}- $(H_2O)_6$@Graphene between graphene sheets from DFT computations were shown in Fig. 4. The radius of hydration structures of Fe^{3+} ions distorted from 3.92 Å to 2.55 Å inbetween two graphene sheets, indicates that size of the hydrated Fe^{3+} ion inbetween two graphene sheets is smaller than that in solution. This result is similar to the behavior of hydrated K^+ in GO membranes reported in our previous study[41]. Furthermore, we noted that this distorted behavior of the hydrated cations is attributed to the strong hydrated cation-π interactions[48,49]. Thus, this makes the sizes of multivalent ions with undistorted hydrated water in bulk solutions larger than the gate size in the GO sheets, resulting in the higher rejection rates of undistorted hydrated ions

Why $ZnSO_4$-controlled GO membranes can realize effective sieving for the other three multivalent ions, while $FeCl_3$-controlled GO membranes cannot? It is very difficult to directly measure the structures of the hydration shells of these ions. Fortunately, we can reasonably assume that the order of the sizes of the hydration shells correlate well with the order of the interlayer spacings. As shown in Fig. 1(d), the order of the interlayer spacing from widest to narrowest is $FeCl_3$> $Pb(NO_3)_2$ > $CuSO_4$ ≈ $ZnSO_4$. In mixed ion solutions, the interlayer spacings of GO membranes controlled by $ZnSO_4$ or $FeCl_3$ keep the order and only differ slightly from the interlayer spacings of GO membranes with pure $ZnSO_4$ or $FeCl_3$ solutions, as shown in Fig. 3 (b), (d). These results clearly demonstrate that the first added multivalent ions can effectively control the spacing in mixed solutions. Since the $ZnSO_4$-controlled GO membranes have the smallest interlayer spacing, the $ZnSO_4$-controlled GO membrane can reject most of the other multivalent

ions used in the present work. In contrast, the $FeCl_3$-controlled GO membranes have the largest interlayer spacing, hence, other ions are able to easily pass through the GO membranes controlled by $FeCl_3$.

Overall, we developed a sort of GO membrane with an ultrahigh water permeance while still maintaining a high rejection rate of multivalent metal ions. In particular, the permeance reaches an unprecedented 75.2 L m^{-2} h^{-1} bar^{-1}, while maintaining the high rejection rate of 99.9%. We note that this is the most permeable membrane with a satisfactory rejection rate for multivalent ions of all state-of-the-art nanofiltration membranes. The ultrahigh water permeances are attributed to the larger interlayer spacings of the GO membranes resulting from the lack of the drying treatment during the fabrication process. The drying treatment is usually used in conventional methods such as the drop-casting method. Moreover, the GO membranes in the present work showed outstanding stability with superior performance. Furthermore, we found that $ZnSO_4$-controlled GO membranes and $FeCl_3$-controlled GO membranes have different rejection performance, because the ions can control and fix the interlayer spacings of the GO membranes, and thus the controlled ions potentially exclude other cations that require a larger interlayer spacing, or allow other hydrated cations with smaller sizes to pass through. Overall, our findings reveals the beauty of GO membranes in the multivalent ions rejection, and represent a facile step toward ultrahigh permeance, effective rejection, and stable performance GO-based membranes for water purification.

Methods

GO Membrane Preparation. GO membranes were prepared from the 7.5 mg/L GO suspensions on the mixed cellulose ester (MCE) substrates under a pressure of 1 bar using vacuum filtration. Then the GO membranes without drying treatment were prepared to conduct the multivalent metal ions rejection experiments. The GO membranes with four thickness of about 100 nm, 200 nm, 400 nm and 800 nm were prepared by using 20 mL, 40 mL, 80 mL and 160 mL of 7.5 mg/L GO suspensions, which were denoted as GO-20, GO-40, GO-80 and GO-160 membranes, respectively.

GO membranes fabricated by conventional drop-casting method were prepared by drop-casting the GO suspension (4 mg/mL, 1 mL) droplets onto a smooth paper substrate. The GO membranes fabricated by conventional drop-casting method were drying thoroughly at 60 ºC for 12 hours. After that, they were peeled off, rinsed and soaked with DI water for more than half an hour to remove the absorbed metal ions, then dried in a dry dish at room temperature for three days. These drop-casting GO membranes were used for ion controlling experiments.

Filtration experiment. 5~500 mg/L different multivalent metal cations ($FeCl_3$, $CuSO_4$, $Pb(NO_3)_2$ or $ZnSO_4$) solutions were added into the feed side after the GO membrane were prepared using vacuum filtration, respectively. Under a pressure of 1 bar, the salt solutions were filtered through GO membranes. Filtrates were collected when the filtration process became steady. Water permeances were calculated by measuring the time required to collect 30 mL filtrate. Rejection rates for the multivalent ions were calculated from the concentration of feed and permeate solution. The water permeance (J_w) and Rejection rate (R) was measured by using the following equation (1) and (2):

$$J_w = \frac{V}{\Delta t \times A \times P} \quad (1)$$

$$R = (1 - \frac{C_p}{C_f}) \times 100\% \quad (2)$$

where J_W is the water permeance (L m^{-2} h^{-1} bar^{-1}), V is the volume of the filtrate (L), A is the effective membrane area (m^2). Δt is the permeation time (h) and the P is the filtration pressure (bar). C_p and C_f are the concentration of permeation and feed ions solution which were measured by inductive coupled plasma-optical emission spectrometry (ICP-OES), respectively.

Adsorption experiment. GO membranes were prepared from 40 mL, 7.5 mg/L GO suspensions on substrates using vacuum filtration. Then, 100 mL, 5 mg/L $FeCl_3$, $Pb(NO_3)_2$, $ZnSO_4$, or $CuSO_4$ solutions were added to the feed side, respectively. These salt solutions under ambient conditions (without vacuum filtration) were stirred with a blender at ~180 RPM. Next, samples were collected at different pre-determined time intervals in 120 min to evaluate the residual salt concentrations of the solutions. We noted that the salt solutions in the feed side permeated very slowly though the GO membranes due to their own gravity, the filtrates were only ~ 5 mL within 120 min. Therefore, the effect of the small volume of filtrates on the salt concentration during the adsorption experiments could be negligible.

The adsorption efficiency (AE) was defined by using the following equation (3):

$$AE = \left(1 - \frac{C_a}{C_o}\right) * 100\% \quad (3)$$

where, C_o and C_a is the initial feed concentration and the concentration of salts after adsorption equilibrium, respectively.

Characterizations. As-prepared GO membranes were characterized by scanning electron microscope (SEM, Hitachi, S-4800) and X-ray diffraction (XRD, Siemens, 08DISCOVER, λ=0.15418 nm). The concentration of ions solutions were determined using PS7800 inductively coupled plasma optical emission spectrometer (ICP-OES).

Calculation Methods. The B3LYP[50,51] method is used to study the intermolecular interactions. For geometry optimizations, the double-ζ basis was employed, and a d-polarization function was added (marked with 6-31 G(d)). The pseudopotential function with Lanl2dz is introduced into the basis set for Fe^{3+} ion. Two graphene surfaces of 15.69 × 12.26 $Å^2$ were used for the DFT study, which were large enough to obtain results with a tolerable error[48]. All calculations were carried out using the Gaussian-09 program[52].

Data availability

The authors declare that all the data supporting the findings of this study are available within the article (and its Supplementary Information file), or available from the corresponding author on reasonable request.

Declarations

Acknowledgements

This work was supported by the National Natural Science Foundation of China (U1832150, 11875236,11974366, 11574339), the Scientific Research and Developed Fund of Zhejiang A&F University (no. 2017FR032). The Authors thank Prof. Guosheng Shi and Prof. Gongping Liu for constructive suggestions.

Author information

Fangfang Dai and Feng Zhou contributed equally to this work.

Author Contributions

H.F. conceived the ideas. L.C. and S.L. designed the experiments and co-wrote the manuscript. F.D. and F.Z. performed the experiments and prepared the data graphs. All authours discussed the results and commented on the manuscript.

Additional information

Supplementary information is available in the online version of the paper. Reprints and permissions information is available online at www.nature.com/reprints. Publisher's note: Springer Nature remains neutral with regard to jurisdictional claims in published maps and institutional affiliations. Correspondence and requests for materials should be addressed to L.C. (liangchen@zafu.edu.cn) and S. L. (liangshanshan@ecust.edu.cn)

Competing interests

The authors declare no competing financial interests.

References

1. Tan, Z., Chen, S., Peng, X., Zhang, L. & Gao, C., Polyamide membranes with nanoscale Turing structures for water purification. *Science* **360** (6388), 518-521 (2018).
2. Homaeigohar, S.& Elbahri, M., Graphene membranes for water desalination. *NPG Asia Materials* **9**, e427 (2017).
3. Werber, J. R., Osuji, C. O.& Elimelech, M., Materials for next-generation desalination and water purification membranes. *Nat. Rev. Mater.* **1**, 16018 (2016).

4. Wang, K., Abdalla, A. A., Khaleel, M. A., Hilal, N., & Khraisheh, M. K., Mechanical properties of water desalination and wastewater treatment membranes. *Desalination* **401**, 190-205 (2017).
5. Mohammad, A.W., Teow, Y. H., Ang, W. L., Chung, Y. T., Oatley-Radcliffe, D. L., & Hilal, N., Nanofiltration membranes review: Recent advances and future prospects. *Desalination* **356**, 226-254 (2015).
6. Wang, Z., Wang, Z., Lin, S., Jin, H., Gao, S., Zhu, Y. & Jin, J., Nanoparticle-templated nanofiltration membranes for ultrahigh performance desalination. *Nat. Commun.* **9** (1), 2004 (2018).
7. Werber, J. R., Deshmukh, A., & Elimelech, M., The Critical Need for Increased Selectivity, Not Increased Water Permeability, for Desalination Membranes. *Environ. Sci. Tech. Let.* **3** (4), 112-120 (2016).
8. Dikin, D. A., Stankovich, S., Zimney, E. J., Piner, R. D., Dommett, G. H. B., Evmenenko, G., Nguyen, S. T. & Ruoff, R. S., Preparation and characterization of graphene oxide paper. *Nature* **448** (7152), 457-460 (2007).
9. Nair, R. R., Wu, H. A., Jayaram, P. N., Grigorieva, I. V. & Geim, A. K., Unimpeded Permeation of Water Through Helium-Leak–Tight Graphene-Based Membranes. *Science* **335** (6067), 442-444 (2012).
10. Joshi, R. K., Carbone, P., Wang, F. C., Kravets, V. G., Su, Y., Grigorieva, I. V., Wu, H. A., Geim, A. K. & Nair, R. R., Precise and Ultrafast Molecular Sieving Through Graphene Oxide Membranes. *Science* **343** (6172), 752-754 (2014).
11. Mi, B. Graphene Oxide Membranes for Ionic and Molecular Sieving. *Science* **343** (6172), 740-742 (2014).
12. Shen, J., Liu, G., Huang, K., Chu, Z., Jin, W. & Xu, N., Subnanometer Two-Dimensional Graphene Oxide Channels for Ultrafast Gas Sieving. *ACS Nano* **10** (3), 3398-3409 (2016).
13. Qi, B., He, X., Zeng, G., Pan, Y., Li, G., Liu, G., Zhang, Y., Chen, W. & Sun, Y., Strict molecular sieving over electrodeposited 2D-interspacing-narrowed graphene oxide membranes. *Nat. Commun.* **8**, 825 (2017).
14. Sun, P., Wang, K., & Zhu, H., Recent Developments in Graphene-Based Membranes: Structure, Mass-Transport Mechanism and Potential Applications. *Adv. Mater.* **28** (12), 2287-2310 (2016).
15. Celebi, K., Buchheim, J., Wyss, R. M., Droudian, A., Gasser, P., Shorubalko, I., Kye, J.-Il, Lee, C., & Park, H. G., Ultimate Permeation Across Atomically Thin Porous Graphene. *Science* **344** (6181), 289-292 (2014).
16. Yeh, C.-N., Raidongia, K., Shao, J., Yang, Q.-H.& Huang, J., On the origin of the stability of graphene oxide membranes in water. *Nat. Chem.* ***7***, 166 (2015).
17. Huang, L., Li, Y., Zhou, Q., Yuan, W.& Shi, G., Graphene Oxide Membranes with Tunable Semipermeability in Organic Solvents. *Adv. Mater.* **27** (25), 3797-3802 (2015).
18. Abraham, J., Vasu, K. S., Williams, C. D., Gopinadhan, K., Su, Y., Cherian, C. T., Dix, J., Prestat, E., Haigh, S. J., Grigorieva, I. V., Carbone, P., Geim, A. K.& Nair, R. R., Tunable sieving of ions using graphene oxide membranes. *Nat. Nanotechnol.* **12**, 546-550 (2017).
19. Morelos-Gomez, A., Cruz-Silva, R., Muramatsu, H., Ortiz-Medina, J., Araki, T., Fukuyo, T., Tejima, S., Takeuchi, K., Hayashi, T., Terrones, M.& Endo, M., Effective NaCl and dye rejection of hybrid graphene

oxide/graphene layered membranes. *Nat. Nanotechnol.* **12**, 1083 (2017).

20. Liang, S., Wang, S., Chen, L., & Fang, H., Controlling interlayer spacings of graphene oxide membranes with cationic for precise sieving of mono-/multi-valent ions. *Sep. Purif. Technol.* **241**, 116738 (2020).
21. Cheng, C., Jiang, G., Garvey, C. J., Wang, Y., Simon, G. P., Liu, J. Z., & Li, D., Ion transport in complex layered graphene-based membranes with tuneable interlayer spacing. *Sci. Adv.* **2** (2), e1501272 (2016).
22. Kim, H. W., Yoon, H. W., Yoon, S.-M., Yoo, B. M., Ahn, B. K., Cho, Y. H., Shin, H. J., Yang, H., Paik, U., Kwon, S., Choi, J.-Y., & Park, H. B., Selective Gas Transport Through Few-Layered Graphene and Graphene Oxide Membranes. *Science* **342** (6154), 91-95(2013).
23. Koenig, S. P. Wang, L., Pellegrino, J., & Bunch, J. S., Selective molecular sieving through porous graphene. *Nat. Nanotechnol.***7** (11), 728-732 (2012).
24. Liu, G., Jin, W. & N. Xu., Graphene-based membrane *Chem. Soc. Rev.* **44**, 5016-5030 (2015).
25. Wang, H., Yang, Y., Liang, Y., Robinson, J. T., Li, Y., Jackson, A., Cui, Y. & Dai, H., Graphene-Wrapped Sulfur Particles as a Rechargeable Lithium-Sulfur Battery Cathode Material with High Capacity and Cycling Stability. *Nano Lett.* **11** (7), 2644-2647 (2011).
26. Lozada-Hidalgo, M., Hu, S., Marshall, O., Mishchenko, A., Grigorenko, A. N., Dryfe, R. A. W., Radha, B., Grigorieva, I. V. & Geim, A. K., Sieving hydrogen isotopes through two-dimensional crystals. *Science* **351** (6268), 68-70 (2016).
27. Sun, P., Zheng, F., Zhu, M., Song, Z., Wang, K., Zhong, M., Wu, D., Little, R. B., Xu, Z. & Zhu, H., Selective Trans-Membrane Transport of Alkali and Alkaline Earth Cations through Graphene Oxide Membranes Based on Cation - π Interactions. *ACS Nano* **8**, 850 (2014).
28. Surwade, S. P., Smirnov, S. N., Vlassiouk, I. V., Unocic, R. R., Veith, G. M., Dai, S. & Mahurin, S. M., Water Desalination Using Nanoporous Single-Layer Graphene. *Nat. Nanotechnol.* **2015, 10**, 459 (2015).
29. Lin, L.-C. & Grossman, J. C., Atomistic understandings of reduced graphene oxide as an ultrathin-film nanoporous membrane for separations. *Nat. Commun.* **6**, 8335 (2015).
30. Hung, W.-S., Tsou, C.-H., De Guzman, M., An Q.-F., Liu, Y.-L., Zhang Y.-M., Hu, C.-C., Lee, K.-R., & Lai, J.-Y., Cross-Linking with Diamine Monomers To Prepare Composite Graphene Oxide-Framework Membranes with Varying d-Spacing. Chem. Mater. **26** (9), 2983-2990 (2014).
31. Esfandiar, A., Radha, B., Wang, F. C., Yang, Q., Hu, S., Garaj, S., Nair, R. R., Geim, A. K., & Gopinadhan, K., Size effect in ion transport through angstrom-scale slits. *Science* **358** (6362), 511-513(2017).
32. O'Hern, S. C., Boutilier, M. S. H., Idrobo, J.-C., Song, Y., Kong, J., Laoui, T., Atieh, M., & Karnik, R., Selective Ionic Transport through Tunable Subnanometer Pores in Single-Layer Graphene Membranes. N*ano Lett.* **14** (3),1234-1241 (2014).
33. Liu, X., Ma, R., Wang, X., Ma, Y., Yang, Y., Zhuang, L., Jehan, R., Chen, J., & Wang, X., Graphene oxide-based materials for efficient removal of heavy metal ions from aqueous solution: A review. *Environ. Pollut.* **252**, 62-73 (2019).

34. Chen, W., Chen, S., Liang, T., Zhang, Q., Fan, Z., Yin, H., Huang, K.-W., Zhang, X., Lai, Z. & Sheng, P., High-flux water desalination with interfacial salt sieving effect in nanoporous carbon composite membranes. *Nat. Nanotechnol.* **13** (4), 345-350 (2018).
35. Han, Y., Xu, Z., Gao, C., Ultrathin Graphene Nanofiltration Membrane for Water Purification. *Adv .Funct. Mater.* **23** (29), 3693-3700 (2013).
36. Wu, C., Liu, S., Wan, Z., Zhng, J., Wang, X., Lu, X., Jia, Y., Hung, W.-S. & Lee, K.-R. Nanofiltration membranes with dually charged composite layer exhibiting super-high multivalent-salt rejetion. *J . Membrane Sci.* **517**, 64-72 (2016).
37. Zhang, M., Guan, K., Ji, Y., Liu, G., Jin, W. & Xu, N., Controllable ion transport by surface-charged graphene oxide membrane. *Nat. Commun.* **10**, 1253 (2019).
38. Han, Y., Jiang, Y., &Gao, C.. High-Flux Graphene Oxide Nanofiltration Membrane Intercalated by Carbon Nanotubes. *ACS Appl. Mater. Interfaces* **7** (15), 8147-8155 (2015).
39. Zhang, Y., Zhang, S.& Chung, T.-S., Nanometric Graphene Oxide Framework Membranes with Enhanced Heavy Metal Removal via Nanofiltration. *Environ. Sci. Technol.* **49** (16), 10235-10242 (2015).
40. Yang, Y., Yang, X., Liang, L., Gao, Y., Cheng, H., Li, X., Zou, M., Ma, R., Yuan, Q. & Duan, X., Large-area graphene-nanomesh/carbon-nanotube hybrid membranes for ionic and molecular nanofiltration. *Science* **364** (6445), 1057-1062 (2019).
41. Chen, L., Shi, G., Shen, J., Peng, B., Zhang, B., Wang, Y., Bian, F., Wang, J., Li, D., Qian, Z., Xu, G., Liu, G., Zeng, J., Zhang, L., Yang, Y., Zhou, G., Wu, M., Jin, W., Li, J. & Fang, H., Ion sieving in graphene oxide membranes via cationic control of interlayer spacing. *Nature* **550**, 380-383 (2017).
42. Gui, L., Dong, J., Fang, W., Zhang, S., Zhou, K., Zhu, Y., Zhang, Y., & Jin, J. Ultrafast Ion Sieving from Honeycomb-like Polyamide Membranes Formed Using Porous Protein Assemblies. *Nano Lett.* **20** (8), 5821-5829 (2020).
43. Hu, R., Zhao, G., He, Y., & Zhu, H. The application feasibility of graphene oxide membranes for pressure-driven desalination in a dead-end flow system. *Desalination.* **477**, 114271 (2020).
44. Yang, Y, Chen, L., Li, D.-Y., Yi R.-B., Mo J.-W., Wu M.-H., & Xu. G., Controllable reduction of graphene oxide by electron-beam irradiation. *RSC Adv.* **9** (7), 3597-3604 (2019).
45. Schniepp, H. C., Li, J. L., McAllister, M. J., Sai, H., Herrera Alonso, M., Adamson, D. H., Prud'homme, R. K., Car, R., Saville D. A. & Aksay, I. A. Functionalized Single Graphene Sheets Derived from Splitting Graphite Oxide, *J. Phys. Chem. B* **110**, 8535 (2006).
46. Gómez-Navarro, C., Weitz, T. R., Bittner, A. M., Scolari, M., Mews, A., Burghard, M. & Kern, K., Electronic Transport Properties of Individual Chemically Reduced Graphene Oxide Sheets. *Nano Lett.* **7**, 3499 (2007).
47. Antony, J. & Grimme S. Structures and interaction energies of stacked graphene-nucleobase complexes. *Phys. Chem. Chem. Phys.* **10** (19), 2722 (2008).
48. Shi, G., Liu, J., Wang, C., Song, B.,Tu, Y., Hu, J.& Fang, H., Ion Enrichment on the Hydrophobic Carbon-based Surface in Aqueous Salt Solutions due to Cation-π Interactions. *Sci. Rep.* **3**, 3436 (2013).

49. Yang, Y., Mu, L., Chen, L., Shi, G., & Fang, H. Precise control of the interlayer spacing between graphene sheets by hydrated cations. *Phys. Chem. Chem. Phys.* **21**(14), 7623-7629 (2019).
50. Becke, A. D., Density-functional exchange-energy approximation with correct asymptotic behavior. *Phys. Rev. A* **38** (6), 3098-3100 (1988).
51. Lee, C., Yang, W., Parr, & R. G., Development of the Colle-Salvetti correlation-energy formula into a functional of the electron density. *Phys. Rev. B* **37** (2),785-789 (1988).
52. Gaussian 09, Revision D. 1, Frisch, M. J., Trucks, G. W., Schlegel, H. B., Scuseria, G. E.,Robb, M. A., Cheeseman, J. R., Scalmani, G., Barone, V., Mennucci, B., Petersson, G. A., Nakatsuji, H., Caricato, M., Li, X., Hratchian, H. P., Izmaylov, A. F., Bloino, J., Zheng, G., Sonnenberg, J. L., Hada, M., Ehara, M., Toyota, K., Fukuda, R., Hasegawa, J., Ishida, M., Nakajima, T., Honda, Y., Kitao, O., Nakai, H., Vreven, T., Montgomery, J. A., Jr., Peralta, J. E., Ogliaro, F., Bearpark, M., Heyd, J. J., Brothers, E., Kudin, K. N., Staroverov, V. N., Kobayashi, R., Normand, J., Raghavachari, K., Rendell, A., Burant, J. C., Iyengar, S. S., Tomasi, J., Cossi, M., Rega, N., Millam, J. M., Klene, M., Knox, J. E., Cross, J. B., Bakken, V., Adamo, C., Jaramillo, J., Gomperts, R., Stratmann, R. E., Yazyev, O., Austin, A. J., Cammi, R., Pomelli, C., Ochterski, J. W., Martin, R. L., Morokuma, K., Zakrzewski, V. G., Voth, G. A., Salvador, P., Dannenberg, J. J., Dapprich, S., Daniels, A. D., Farkas, Ö., Foresman, J. B., Ortiz, J. V., Cioslowski, J., Fox, D. J. Gaussian, Inc., Wallingford CT, 2009.

Figures

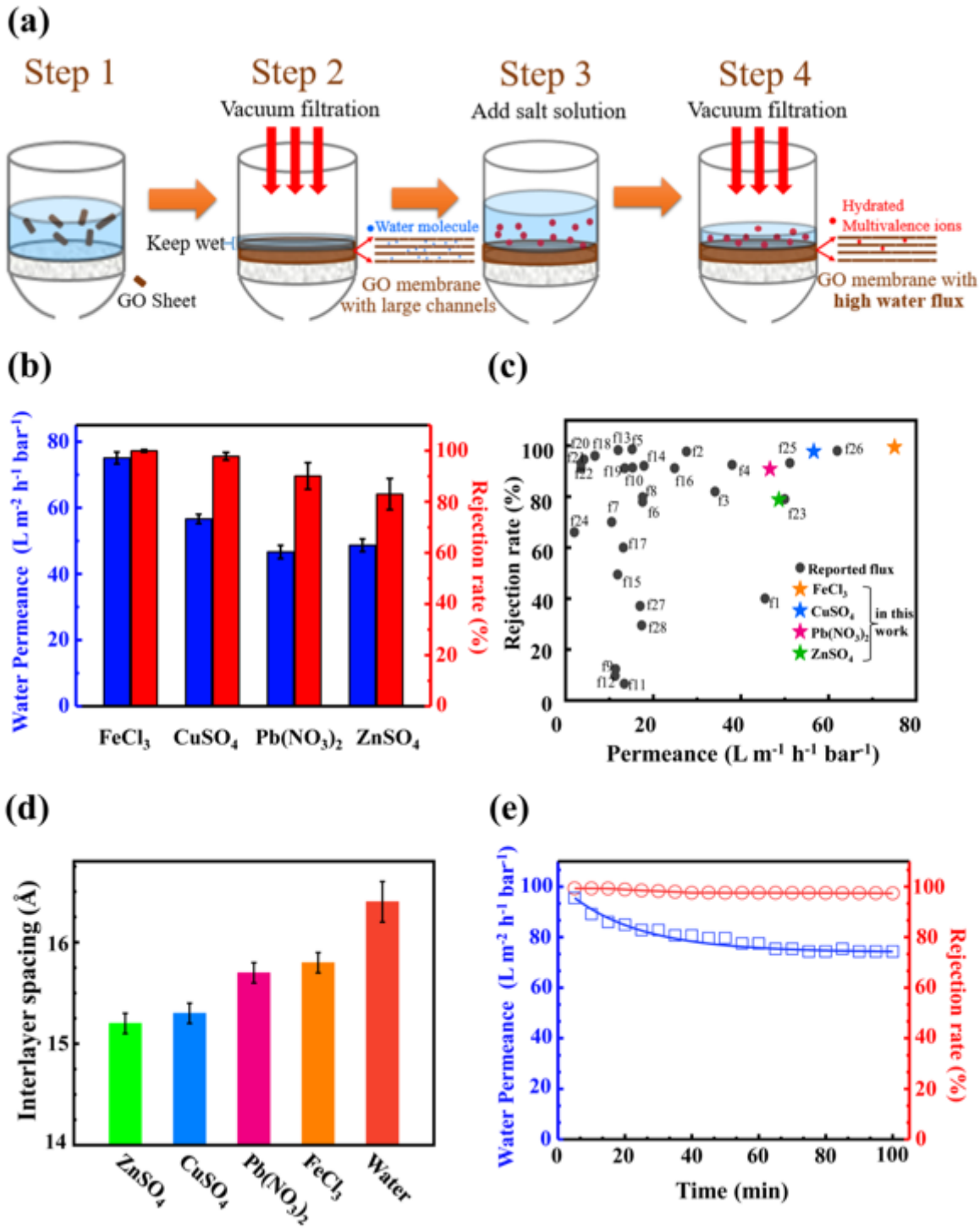

Figure 1

Water treatment performance of the GO membranes for multivalent metal ions. (a) A schematic of the experimental process. (b) Water permeances and rejection rates for the GO membranes with different multivalent ions. (c) Summary of the filtration performance of state-of-the-art membranes reported in the literature based on water permeances and rejection rates for multivalent ions (f1-f28 marked as gray circles, details shown in Supplementary Table S1 in Supporting Information). (d) Interlayer spacings of the GO membranes immersed in different multivalent ion solutions. Error bars indicate the standard

deviation from three different samples. (e) Variations of water permeance and rejection rate of 5 mg/L FeCl3 solution through GO membranes as a function of filtration time. Blue and red lines correspond to water permeances and rejection rates, respectively.

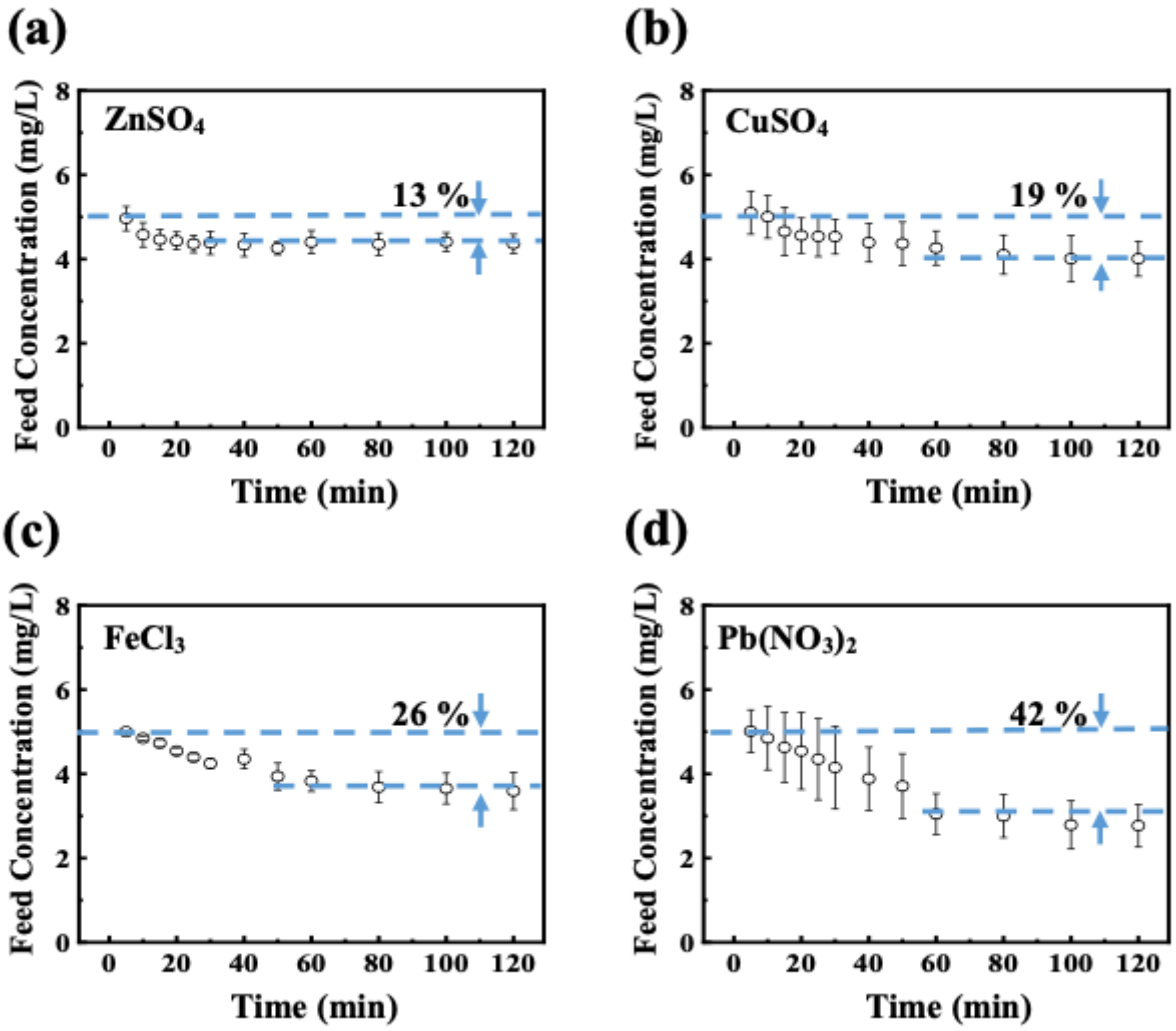

Figure 2

Concentration variations of 5 mg/L (a) ZnSO4, (b) CuSO4, (c) FeCl3, and (d) Pb(NO3)2 solutions adsorbed by the GO membranes as a function of adsorption time.

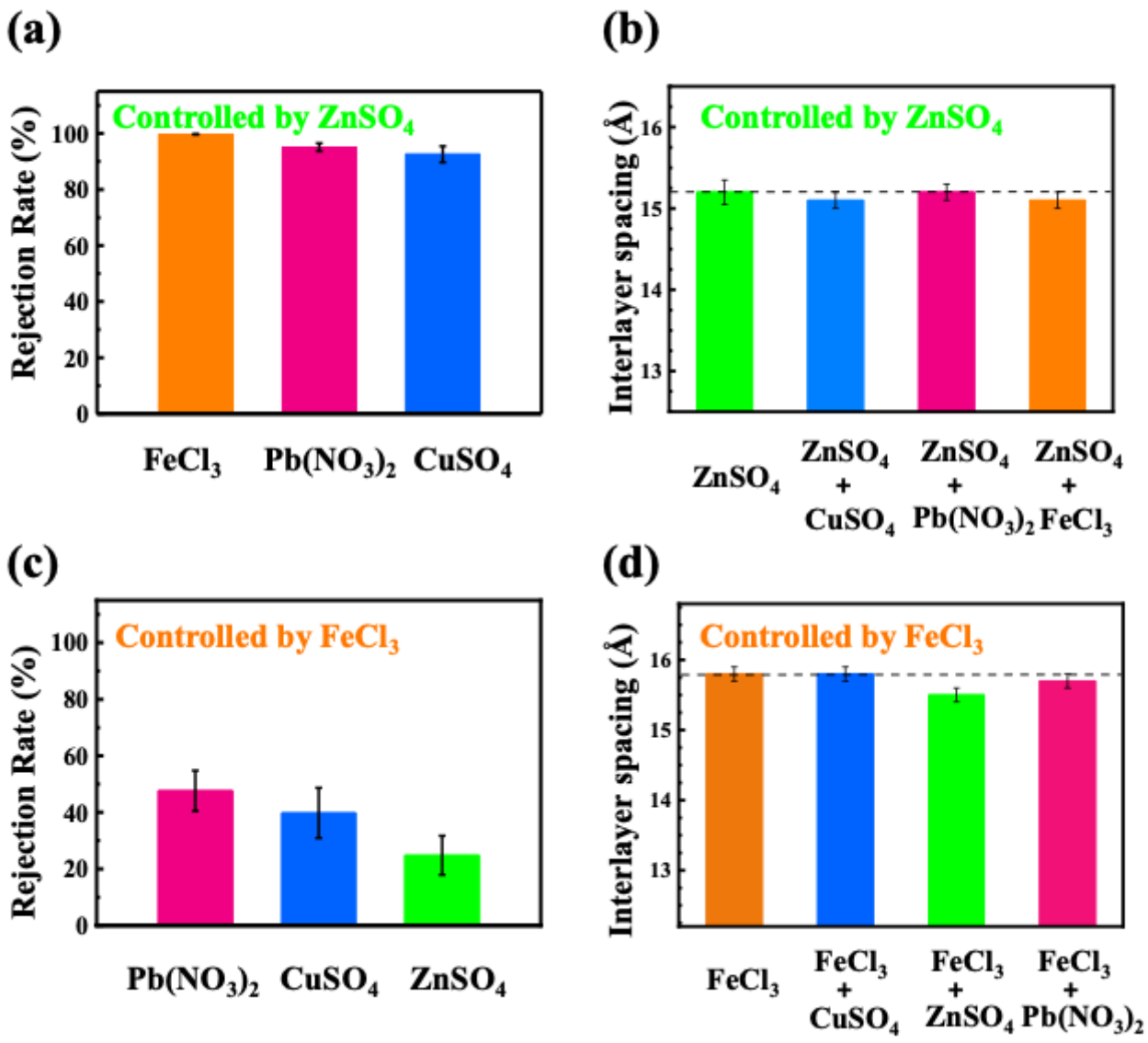

Figure 3

Rejection performance and interlayer spacings in ZnSO4-and FeCl3-controlled GO membranes. (a) and (b) Controlled by ZnSO4. (c) and (d) Controlled by FeCl3. Error bars indicate the standard deviation from three different samples.

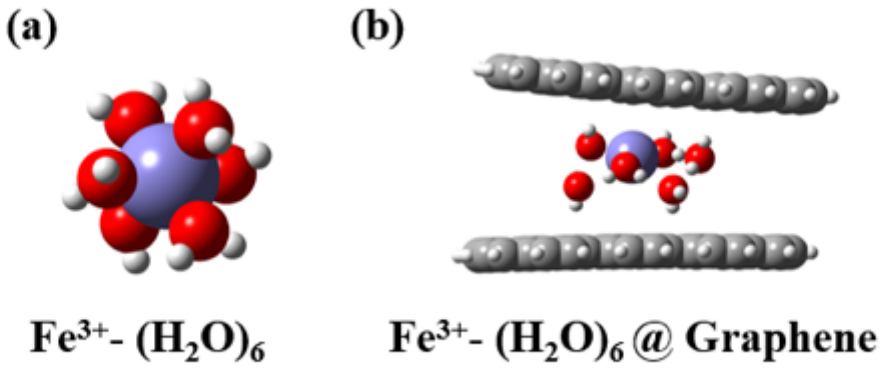

Figure 4

The most stable optimized geometries of the hydrated Fe3+- (H2O)6 and hydrated Fe3+-(H2O)6 @ Graphene from density functional theory computations.

Supplementary Files

This is a list of supplementary files associated with this preprint. Click to download.

- RevisedSupportingInformation.docx